Precision Spectroscopy of X-rays from Antiprotonic Hydrogen

D. F. Anagnostopoulos[1,2], M. Augsburger[3], G. Borchert[1], C. Castelli[4], D. Chatellard[3], P. El-Khoury[5], J.-P. Egger[3], H. Gorke[1], D. Gotta[⋆1], P. Hauser[6], P. Indelicato[5], K. Kirch[6], S. Lenz[1], N. Nelms[4], K. Rashid[7], Th. Siems[1], and L. M. Simons[6]

[1] Institut für Kernphysik, Forschungszentrum Jülich, D-52425 Jülich, Germany
[2] Department of Material Science, University of Ioannina, GR-45110 Ioannina, Greece
[3] Institut de Physique de l'Université de Neuchâtel, CH-2000 Neuchâtel, Switzerland
[4] Department of Physics and Astronomy, University of Leicester, Leicester LEI 7RH, England
[5] Laboratoire Kastler-Brossel, Université Pierre et Marie Curie, F-75252 Paris, France
[6] Paul-Scherrer-Institut (PSI), CH-5232 Villigen, Switzerland
[7] Quaid-I-Azam University, Islamabad, Pakistan

Abstract. Lyman and Balmer transitions of antiprotonic hydrogen and deuterium have been measured at the Low-Energy Antiproton Ring LEAR at CERN in order to determine the strong-interaction effects. In LEAR experiment PS207, the X-rays were detected using Charge-Coupled Devices (CCDs) and a reflection-type crystal spectrometer. A complete set of strong-interaction parameters for the $1s$ and the $2p$ levels is now available for both $\bar{p}H$ and $\bar{p}D$ after evidence was found for the $\bar{p}D$ Kα transition.

1 Introduction

The hadronic shifts and broadenings of the atomic s and p levels in an antiprotonic atom are directly related to the complex scattering lengths and volumes of the antiproton-nucleus system [1,2]. Therefore, the spectroscopy of the low-lying X-ray transitions is equivalent to a scattering experiment at relative energy zero (Fig. 1). The measurement of antiprotonic hydrogen explicitly tests the long range part of the $\bar{N}N$ interaction [3,4,5,6]. The results have to be consistent with the values obtained from extrapolation to threshold of the low-energy scattering experiments [7,8], and also have to show a normal threshold behavior if no nearby resonances exist [9].

In a first generation of LEAR experiments, K transitions from $\bar{p}H$ were detected by using conventional solid-state and gas-filled devices. The weighted average of results from the experiments PS174 [10,11] and PS175 [12] reached an accuracy of 3% and 6% for the spin-averaged shift ϵ_{1s} and broadening Γ_{1s}, respectively. The knowledge from individual hyperfine states strongly enhances the sensitivity to the various theoretical approaches for the hadronic interaction, but

⋆ corresponding author

spin-dependent information – for the $^1S_0$ (PS171 [13]) and the $^3S_1$ (PS175 [12]) states – could be only obtained with additional assumptions.

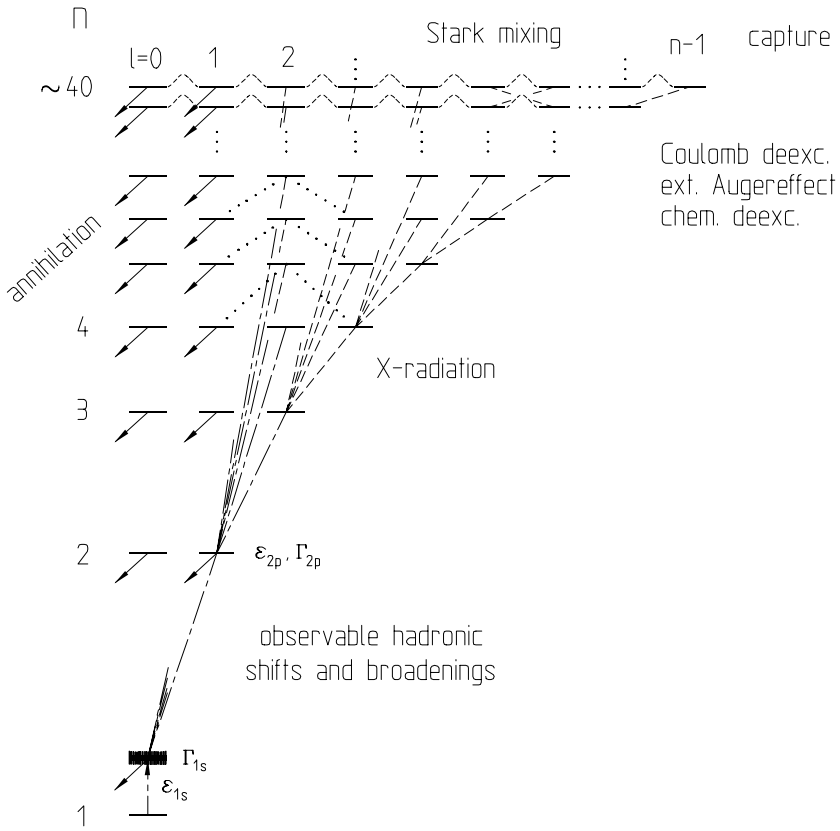

Fig. 1. Atomic cascade in antiprotonic hydrogen. The hadronic interaction is observed by a level shift and a broadening of the low-lying atomic levels as compared to the calculated binding energies and radiative decay widths assuming a pure electromagnetic interaction

The spin-averaged $2p$-level broadening Γ_{2p} in $\bar{p}H$ was determined indirectly from the intensity balance between the total Balmer series and the Lyman α transition [10,12], a method which is, however, only strictly valid in the limit of equal widths for all $2p$ hyperfine levels [8,12,14]. No hadronic effects were observed in antiprotonic deuterium because of the weakness of the K transitions due to the enhanced absorption from the $\bar{p}D$ $l = 1$ states.

The goal of LEAR experiment PS207 [15] was to extend the information on the $\bar{N}N$ interaction

- by a direct measurement of the $2p$ level strong-interaction shift and broadening both in antiprotonic hydrogen and deuterium with a crystal spectrom-

eter, which is necessary to achieve an accuracy of a few 10^{-6} for the energy measurement of the Balmer α transitions (Table 1) together with an energy resolution of 10^{-4}, and

- to improve the results derived from the $np - 1s$ ground-state transitions by using Charge-Coupled Devices (CCDs), which were applied for the first time to measurements of antiprotonic X-rays.

2 Experiment

For the use of high-resolution crystal spectrometers and semiconductor detectors, both a concentrated stop volume and – to obtain sufficiently high line yields – dilute gas targets are mandatory [10,12,16]. Such conditions can be achieved with the cyclotron trap [17]. Almost the full beam extracted from LEAR of up to 10^6 antiprotons per second with 105 MeV/c momentum was stopped, forming a concentrated source of antiprotonic X-rays with a diameter of 20 mm at a pressure of 20 mbar H_2. Under these conditions, the line yield of the Balmer α transitions in the hydrogen isotopes reaches almost 50%. Owing to the strong p-wave annihilation, the Lyman α yield is only of the order of 1% for $\bar{p}H$ [12].

To use the LEAR beam efficiently, the crystal spectrometer was set up as a twin system for the $\bar{p}H$ experiment. Three independent spherically-bent quartz crystals of 100 mm (Fig. 2) were used. Each of the crystals was directed to its own CCD detector in order to avoid any reduction of resolution from the matching of reflections. About 30 Balmer α events per hour were recorded per crystal-detector system in the case of hydrogen. For antiprotonic deuterium with a single crystal-detector system a count rate of about 60 per hour was achieved in spite of the smaller sensitive area of the detector (Table 2) because of less absorption.

Table 1. Calculated electromagnetic energies and line widths of the antiprotonic transitions measured with the crystal spectrometer. The energy resolution ΔE_{exp} of the Bragg spectrometer was determined from narrow transitions of antiprotonic noble gases. Θ_B stands for the Bragg angle

transition	E_{QED} (eV)	Γ_{QED} (meV)		crystal	reflection	Θ_B	ΔE_{exp} (meV)
$\bar{p}^3He(5g-4f)$	1686.477	0.26	[18]	quartz	100	59.8°	286±7
$\bar{p}H(3d-2p)$	1736.798	0.38	[18]	quartz	100	57.0°	
Si Kα_1	1739.986±0.019	0.524±0.035	[19,20]	quartz	100	56.9°	
$\bar{p}^4He(5g-4f)$	1797.582	0.28	[18]	quartz	100	54.1°	262±49
S Kα_1	2307.89±0.03	0.769±0.026	[19,20]	silicon	111	56.9°	
$\bar{p}D(3d-2p)$	2316.483	0.51	[18]	silicon	111	58.6°	
$\bar{p}^{20}Ne(13p-12o)$	2444.035	10	[18]	silicon	111	54.0°	333±34

The energy calibration was obtained with Si and S Kα fluorescence X-rays excited by means of an X-ray tube. Because the natural widths of the fluorescence X-rays exceed the experimental resolution at least by a factor of two, the response function of the spectrometer was determined from the narrow antiprotonic transitions $\bar{p}He(5g-4f)$ and $\bar{p}Ne(13p-12o)$, lines which are not affected by the strong interaction. For the 1.7 keV Balmer α transition from $\bar{p}H$, quartz crystals are the only possible choice for the Bragg crystal. The theoretical limit for the resolution of 180 meV was missed by a factor of 1.7 (Table 1). In the case of $\bar{p}D$, a silicon crystal was used because of its higher reflectivity. Here, the theoretical limit for the resolution of 360 meV was reached [21].

The CCDs for the direct measurement of the antiprotonic X-rays were installed in the second bore hole of the cyclotron trap close to the stop volume. Thus, a few per mille of the full solid angle were covered. The relative efficiency and the in-beam resolution function were obtained in a separate measurement from the saturated X-ray transitions in $\bar{p}N$. Two different types of CCDs were used: (i) MOS CCDs with a typical depletion depth of about 30 μm [22,23] and (ii) the prototype of a high-rate X-ray detector based on a fully depleted (290 μm) pn-CCD [24].

Table 2. CCD parameters. In the $\bar{p}H(3d-2p)$ measurement, one CCD detector was used for each of the three crystals (see Fig. 2)

transition	CCD type	pixel size	no. of pixels	energy resolution	
$\bar{p}H(np-1s)$	MOS	22μm	3 × 385 × 576	320 eV @ 8 keV	direct measurement
	pn-CCD	150 μm	1 × 64 × 64	240 eV @ 8 keV	direct measurement
$\bar{p}D(np-1s)$	MOS	22 μm	3 × 385 × 576	320 eV @ 8 keV	direct measurement
$\bar{p}H(3d-2p)$	MOS	22.5 μm	4 × 770 × 576	160 eV @ 1.7 keV	crystal spectrometer
	MOS	27 μm	1 × 820 × 1024	130 eV @ 1.7 keV	crystal spectrometer
$\bar{p}D(3d-2p)$	MOS	22.5 μm	2 × 770 × 576	140 eV @ 2.3 keV	crystal spectrometer

3 Results

3.1 Spin-averaged shifts and widths

1s ground-state

The results using CCDs for the direct measurement of X-rays from $\bar{p}H$ [22] were consistent with the values obtained from the earlier experiments mentioned above. The superior background-suppression capabilities of the pixel devices led to an improvement of the peak-to-background ratio (Fig. 3). The new world-average values for the strong-interaction effects are listed in Table 3 together with typical results from model calculations.

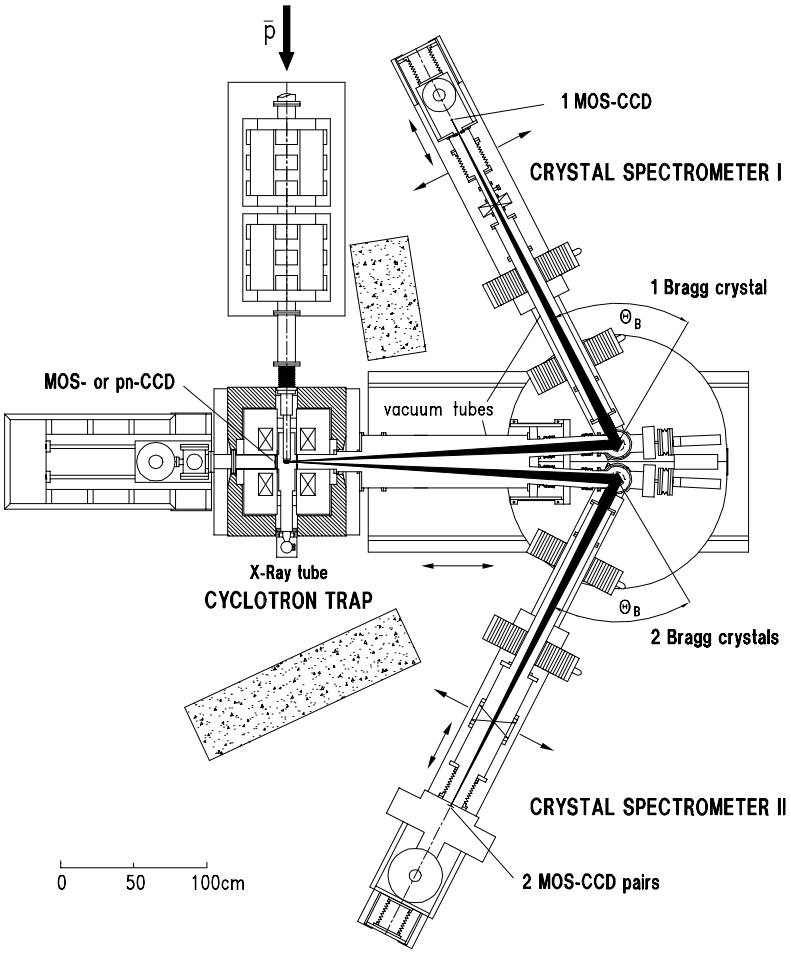

Fig. 2. Set-up of cyclotron trap, crystal spectrometer, and CCD detectors in LEAR experiment PS207. For the $\bar{p}H$ measurement, the two-arm crystal spectrometer was equipped in total with 3 spherically-bent quartz crystals each reflecting to a separate X-ray detector. Further CCD detectors installed in the second bore hole of the cyclotron trap were used for direct measurements of antiprotonic X-rays

For the first time, evidence was found for the $\bar{p}D$ Lyman α transition [23]. The low yield (Fig. 3) and the width of the transition are in line with the strong annihilation from the $2p$ levels in hydrogen and deuterium as observed in the experiment using the crystal spectrometer. A simple scaling relation, based on the geometrical overlap of wave functions, yields $\Gamma_{1s}^{\bar{p}D} = 2.3 \pm 0.3\,\mathrm{meV}$ [21], a value which is consistent with the direct measurement.

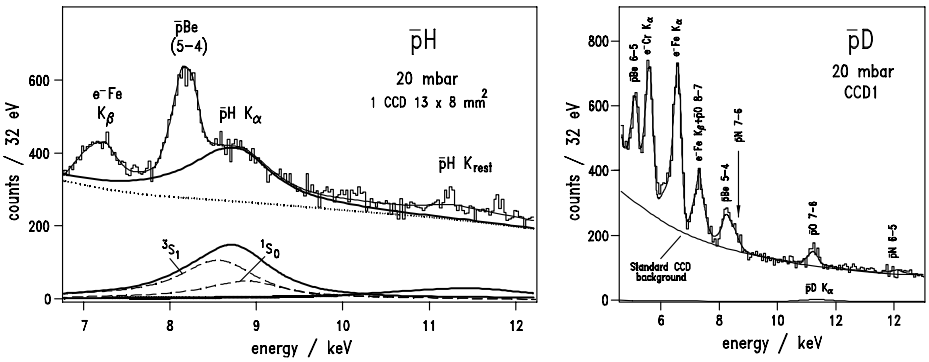

Fig. 3. X-ray spectrum in the energy range of the $\bar{p}H(np-1s)$ transitions as measured with MOS CCDs. The pure electromagnetic transition energies for the $2p-1s$ transitions of the hydrogen isotopes are 9405.7 keV and 12.505 keV

2p state

For $\bar{p}H$, the new world average of the $2p-$level width, derived from the intensity balance, is $\Gamma_{2p}^{bal} = 32.5 \pm 2.1$ meV. The small error achieved for this quantity combined with the width of the 2^3P_0 hyperfine state as measured with the crystal spectrometer allows to correct for the different annihilation widths from the $2p$ sublevels. The corrected value Γ_{2p} (see Table 3) deviates significantly from Γ_{2p}^{bal} due to the large width of the 2^3P_0 state [21] and is now in good agreement with low-energy scattering experiments [8].

In the case of $\bar{p}D$, the spin-averaged hadronic broadening is derived from a fit to the line shape using a single Lorentzian and taking into account the spectrometer response function as measured with $\bar{p}Ne$. The broadening found is in agreement with results from a multiple-scattering ansatz, whereas the shift is underestimated by this model [25]. No evidence was found for a hyperfine splitting (see below).

3.2 Hyperfine structure

1s ground state in $\bar{p}H$

About 20000 Kα events were recorded, which did not allow to determine unbiased the individual hyperfine components with an accuracy comparable to the one of the spin-averaged values. The errors for the $^3S_1$ hyperfine state are of the order of 10% for the shift and 15% for the broadening and are consistent with the values given in [12] (Table 4). Parameters for the less intense $^1S_0$ state could be obtained if the $^3S_1/^1S_0$ intensity ratio was fixed for the fit in accordance with reasonable assumptions for the different $2p$-level widths [22]. An unbiased fit yields errors of the order of at least 50%.

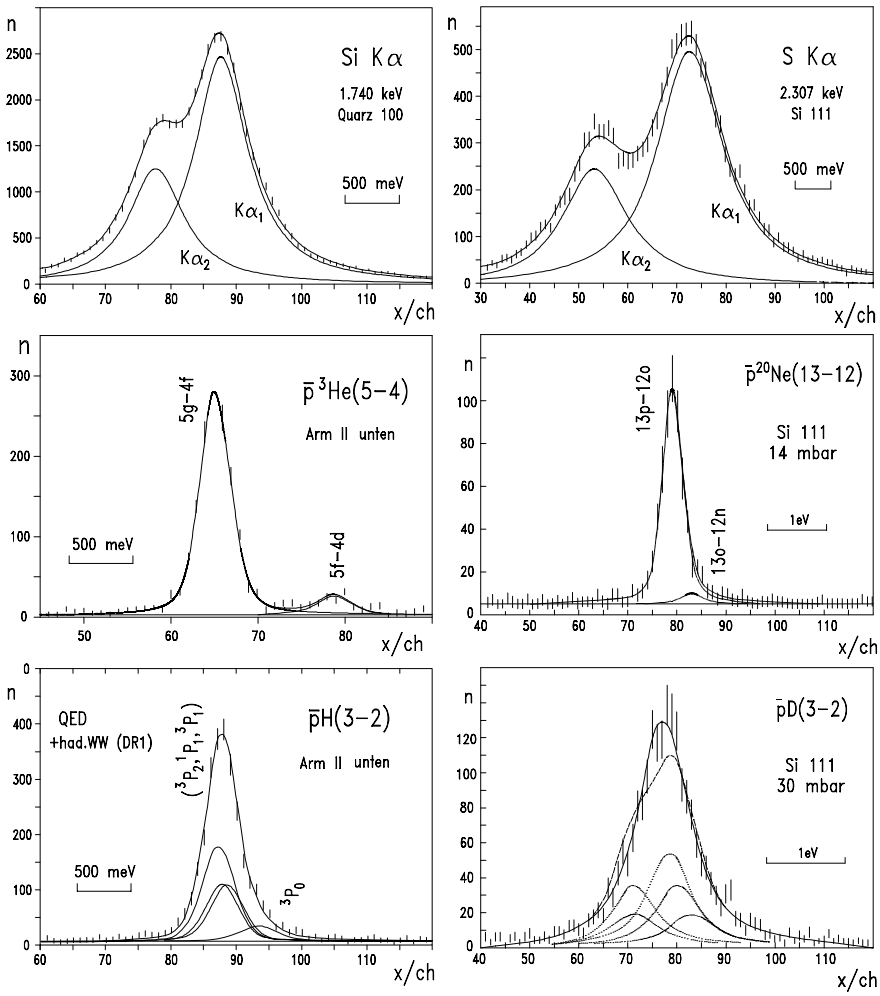

Fig. 4. Position spectra of silicon and sulphur Kα fluorescence lines, the transitions $\bar{p}^3He$ and $\bar{p}Ne$ used to determine the crystal spectrometer response function, and the Balmer α lines from the hydrogen isotopes. For $\bar{p}^3He$, the parallel transition $(5f-4d)$ is well resolved from the circular transitions $(5g-4f)$

2p states in $\bar{p}H$ and $\bar{p}D$

Hadronic effects for $l \geq 2$ states are negligibly small [5]. Therefore, the $2p$ hyperfine levels are assumed to be populated according to their statistical weight.

The determination of the hadronic effects relies on the knowledge of the electromagnetic energy levels, especially if not all components are resolved (Fig. 4). However, the results of the various calculations both for hydrogen and deuterium [18,26,27] differ considerably. Here, only the values from the most recent

Table 3. World averages of experimental results for the spin–averaged hadronic shifts and broadenings in antiprotonic hydrogen and deuterium in comparison with predictions. The + (–) sign for the shift stands for an attractive (repulsive) interaction. The errors for ϵ_{2p} include the uncertainties of the Kα energies of Si and S. The calculations labeled DR1 and KW use the same parametrization for the real part of the $\bar{N}N$ potential, but different approaches for the absorptive part

			ϵ_{1s} (eV)	Γ_{1s} (eV)		ϵ_{2p} (meV)	Γ_{2p} (meV)	
$\bar{p}H$	experiment		-714 ± 14	1097 ± 42	[22]	$+15 \pm 20$	38.0 ± 2.8	[21]
	theory	DR1	-707	933	[5]	$+6$	33.5	[5]
		KW	-698	1062	[5]	$+7$	35	[5]
		eff. range	-600	1080	[7]	$+9$	39	[7]
$\bar{p}D$	experiment		-1050 ± 250	1100 ± 750	[23]	-243 ± 26	489 ± 30	[21]
	theory	mult. scatt.	≈ -4000	≈ 5500	[25]	-52	422	[25]
		3-body cal.	≈ -1600	≈ 1000	[28]			
		potential cal.	≈ -4000	≈ 2000	[29]			

Table 4. Hadronic parameters of individual hyperfine states in $\bar{p}H$

28	1^1S_0		1^3S_1		2^3P_0
ϵ	-440 ± 75 eV	-740 ± 150 eV	-785 ± 35 eV	-850 ± 42 eV	$+139 \pm 38$ meV
Γ	1200 ± 250 eV	1600 ± 400 eV	940 ± 80 eV	770 ± 150 eV	120 ± 25 meV
	[22]	[13]	[22]	[12]	[21]

calculation [18] (labeled **new** in Fig. 5) were used for the reason discussed below and in [16,21]. To illustrate the size of the strong-interaction shifts $\epsilon_{\rm had}$, results from model calculations for $\bar{p}H$ [5] and $\bar{p}D$ [25] are also shown in Fig. 5.

In the case of $\bar{p}D$, the line shape could not be understood if the analysis is based on the prediction of [26] for the electromagnetic level splitting. According to this calculation, the electromagnetic interaction dominates the splitting in a way that the $3d-2p$ line shape is approximately a "doublet" structure formed by the groups ($^4P_{3/2}$,$^4P_{1/2}$,$^4P_{1/2}$) and ($^4P_{5/2}$,$^2P_{3/2}$,$^2P_{1/2}$) (Fig. 5: **old**). The measured line shape, however, does not show any evidence for such a "doublet" structure [21] (Fig. 4: asymmetric fit to the line shape using the 5 displayed hyperfine components).

The discrepancy between observed and expected line shape actually provoked a recalculation for the level splitting both in hydrogen and deuterium, which yields much smaller splittings [18] (Fig. 5: new). Hence, the strong-interaction parameters are then found from a single-line fit as mentioned above (Fig. 4: symmetric fit).

In hydrogen, the 2^3P_0 hyperfine state plays a particular role. Its electromagnetic splitting of more than 200 meV is predicted to be increased by another 100 meV by the long-range $\bar{p}p$ potential. In fact, the line profile of the $3d-2p$ transition exhibits a shoulder at the high energy side (Fig. 4), which is

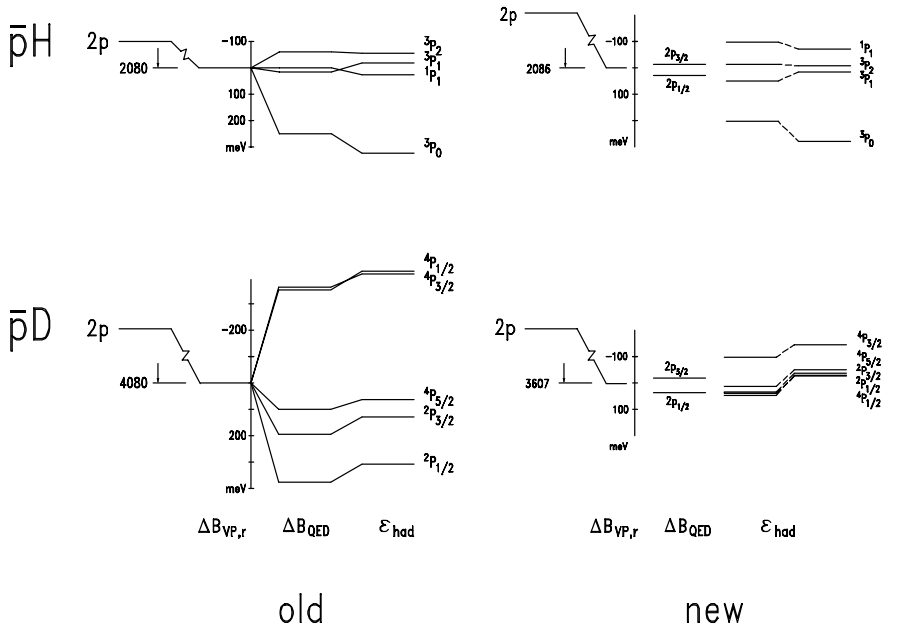

Fig. 5. Comparison of (former and recent) calculations for the electromagnetic hyperfine splittings. The calculations include vacuum polarization ΔB_{VP}, electromagnetic fine ΔB_{FS} and hyperfine structure ΔB_{HFS}

interpreted as the 2^3P_0 state (Table 4 and Fig. 5). The close-lying components 2^3P_2, 2^3P_1, and 2^1P_1 are not resolved . The large value for the hadronic shift $\epsilon(2^3P_0)$ even exceeds the results obtained from most of the theoretical calculations. The broadening $\Gamma(2^3P_0)$ – much larger than the spin-averaged value – is in the range of the predictions as are the measured mean shift and width of the group (2^3P_2,2^3P_1,2^1P_1).

4 Summary and outlook

The spin-averaged hadronic shifts and widths of the $1s$ and the $2p$ state have been measured both for antiprotonic hydrogen and deuterium. Furthermore, information on individual hyperfine states was obtained for $\bar{p}H$. Here, the strong-interaction parameters of the 2^3P_0 hyperfine state could be determined using a crystal spectrometer. The hadronic effects in the 1^1S_0 and 1^3S_1 hyperfine ground states were derived with the help of a few assumptions.

The experimental results support the meson-exchange model, which is used to derive the real part of the long- and medium-range $\bar{N}N$ potential. There is no need for exotic $\bar{p}p$ bound states close to threshold. The poor accuracy concerning the individual hyperfine states 1^1S_0 and 1^3S_1 of $\bar{p}H$ in an unbiased analysis

remains unsatisfactory, because this limits a sensible discrimination between various approaches in the framework of the meson-exchange model.

A remeasurement of the Lyman transitions from $\bar{p}H$ and the search in $\bar{p}D$ with the forthcoming generation of CCD detectors is desirable. Such a measurement requires a continuous antiproton beam of the order of $10^5\bar{p}/s$, which at present is not available directly from the Antiproton Decelerator facility (AD) at CERN [30]. Installing either a slow extraction scheme for the AD or forming a beam by reaccelerating antiprotons at the exit of a catcher trap, as foreseen e. g. in the ASACUSA experiment [31], may offer a chance to continue on the $\bar{N}N$ strong-interaction studies terminated by the shut-down of LEAR. Such an experiment should be able to improve on the accuracy by a factor of at least 5 for $\bar{p}H$ and to confirm the existence of the $\bar{p}D$ ground-state transition.

References

1. S. Deser et al.: Phys. Rev. **96**, 774 (1954)
2. T. L. Trueman: Nucl. Phys. **26**, 57 (1961)
3. W. W. Buck, C. B. Dover, and J. M. Richard: Ann. of Phys. **121**, 47 (1979)
4. C. B. Dover and J. M. Richard: Phys. Rev. C **21**, 1466 (1980)
5. J. Carbonell, G. Ihle, and J. M. Richard: Z. Phys. A **334**, 329 (1989)
6. J. Carbonell, J.-M. Richard, and S. Wycech: Z. Phys. A **343**, 325 (1992)
7. I. L. Grach, B. O. Kerbikov, and Yu. A. Simonov: Sov. J. Nucl. Phys. **48**, 609 (1988)
8. K. V. Protasov et al.: Eur. Phys. J. A **7**, 429 (2000)
9. D. Dalkarov, K. Protasov, and I. Shapiro: Int. Jour. of Mod. Phys. A **5**, no. 11, 2155 (1990)
10. C. A. Baker et al.: Nucl. Phys. A **483**, 631 (1988)
11. C. W. E. Eijk et al.: Nucl. Phys. A **486**, 604 (1988)
12. K. Heitlinger et al.: Z. Phys. A **342**, 359 (1992)
13. M. Ziegler et al.: Phys. Lett. **206** B, 151 (1988)
14. C. J. Batty: Rep. Prog. Phys. **52**, 1665 (1989)
15. D. Anagnostopoulos et al.: LEAR experiment PS207, CERN/PSCC/90-9/P124 (1990)
16. D. Gotta: 'Experiments on Exotic Atom Spectroscopy'. In: *Frontier Tests of QED and Physics of the Vacuum*, ed. by E. Zavattini, D. Bakalov, C. Rizzi (Heron Press, Sofia 1998) pp. 170–185
17. L. M. Simons: Physica scripta **T22**, 90 (1988); Hyperfine Interactions **81**, 253 (1993)
18. S. Boucard and P. Indelicato (private communication)
19. R. Deslattes and T. Mooney (private communication)
20. R. Deslattes et al.: in *Atomic and Molecular Data and Their Applications*, edited by P. Mohr and W. L. Wiese, AIP 1-56396-751-0/98 (1998), pp. 89–103
21. D. Gotta et al.: Nucl. Phys. A **660**, 283 (1999)
22. M. Augsburger et al.: Nucl. Phys. A **658**, 149 (1999)
23. M. Augsburger et al.: Phys. Lett. B **461, 417** (1999)
24. H. Gorke: Entwicklung eines Hochraten-CCDs zur Messung der Röntgenstrahlung antiprotonischer Atome. Thesis, University of Cologne (1996)
25. S. Wycech, A. M. Green, and J. A. Niskanen: Phys. Lett. **152** B, 308 (1985)
26. S. Barmo, H. Pilkuhn and H. G. Schlaile: Z. Phys. A **301**, 283 (1981)

27. E. Borie: In: *Physics at LEAR with Low-Energy Cooled Antiprotons, 2nd LEAR Workshop, Erice, Italy, 1982*, ed. by U. Gastaldi, R. Klapisch (Plenum, New York 1984) pp. 561–566
28. G. P. Latta and P. C. Tandy: Phys. Rev. C **42**, R1207 (1990)
29. G. Q. Liu, J.-M. Richard, and S. Wycech: Phys. Lett. B **260**,15 (1991)
30. S. Baird et al.: AD design study, CERN/PS/96-43 (AR) (1996) J. Y. Hémery and S. Maury: In: *Low.Energy Antiproton Physics (LEAP 98) Fifth Biennial Conference on Low-Energy Antiproton Physics, Villasimius, Sardinia, Italy, 1998*, ed. C. Cicalò, A. de Falco, G. Puddu, Nucl. Phys. A **655**, 345c (1999)
31. T. Azuma et al.: ASACUSA proposal, CERN/SPSC/97-19/P-307 (1997)